CAATGTTC-3′; CNS-11 reverse, 5′-CTGTCANAGC-CACACAGAAG3′; CNS-12 forward, 5′-TCCACATTT-TCTTNCCTTTG-3′; CNS-12 reverse, 5′-GTNTCNCT-GCCCTTTGATG-3′; CNS-13 forward, 5′-GGNTGAGA-TNCTGGAGGCTC-3′; CNS-13 reverse, 5′-GAGCAG-GTCTGACNNGGGTG-3′; CNS-14 forward, 5′-TTG-GCAATTCCCCTGAAA C-3′; CNS-14 reverse, 5′-AAGCTKAGYTCTGGCAGG-3′; CNS-15 forward, 5′-AAGNNTGTT GCTANGGTCACTGTG-3′; CNS-15 reverse, 5′-GCAGNTGTGGTTTTGAGANGTTCA T-3′; CNS-16 forward, 5′-CTCCCACATCCTTGGGAGGG-3′; and CNS-16 reverse, 5′-CCAGNAGCCAGGGACA-CACC-3′. Amplified PCR products were analyzed by gel electrophoresis on 3% Nusieve GTG agarose gels (BioWhittaker Molecular Applications, Rockland, ME), extracted with QIAquick Gel Extraction Kits (QIAGEN, Valencia, CA), and sequenced with Big Dye chemistry (PE Applied Biosystems, Foster City, CA).

13. Human genomic DNA (8 μg) (catalog number 6550-1 from Clontech Laboratories) was digested (with Pst I, Msp I, Bgl II, Pst I, and Taq$^{\alpha}$I), separated in an 0.8% agarose gel, transferred onto membrane (Hybond N$^+$, Amersham), hybridized at 52°C overnight in Church Buffer [0.5 M $NaHPO_4$ (pH 7.2), 1 mM EDTA, 7% SDS, and 1% bovine serum albumin] with the most stringent wash at 58°C [0.04 M $NaHPO_4$ (pH 7.2), 1 mM EDTA, and 1% SDS]. Probes were generated by PCR amplification of human genomic DNA using primer pairs of each CNS element and then gel purified (*12*). A CNS element was defined as single copy if none of the five lanes containing DNA (one of each restriction digest) had more than one or two bands (assumed to be a polymorphism).
14. Gridded high-density dog and baboon libraries (BACPAC Resources, Roswell Park Cancer Institute, Buffalo, NY) were screened by hybridization with CNS-1 probes generated by PCR amplification of dog and human genomic DNA (*12*), respectively. Content mapping of 9 dog BACs and 14 baboon BACs for the presence of *KIF3A*, CNS-2, *IL-4*, CNS-1, *IL-13*, and *RAD50* by PCR defined the location of CNS-1 to the *IL-4* through *IL-13* region.
15. CNS-1 sequences (human, mouse, dog, rat, cow, and rabbit) were searched (the Transcription Factor Database is available at http://transfac.gbf-braunschweig.de/TRANSFAC/index.html) for consensus binding sites of four proteins [NF-AT (nuclear factor of activated T cells), c-maf, GATA-3, and STAT6 (signal transducer and activator of transcription 6)] known to regulate *IL-4* transcription. No conserved consensus binding sites were found.
16. N. Takemoto *et al.*, *Int. Immunol.* **10**, 1981 (1998); S. Agarwal and A. Rao, *Immunity* **9**, 765 (1998).
17. YAC A94G6 (450 kb) (*6*) was retrofitted with pLys2neo vector (gift from K. Peterson) as described [B. C. Lewis, N. P. Shah, B. S. Braun, C. T. Denny, *Genet. Anal. Tech. Appl.* **9**, 86 (1992)]. The yeast shuttling vector, pRS406.CNS-1.*loxP*, was constructed as follows: A 2.4-kb Sac I fragment containing human CNS-1 was cloned into pRS406 (Stratagene) to generate pRS406.CNS-1. Oligonucleotides, LoxP–Pml I (forward 5′-GTGTAACTTCGTATAGCATACAT-TATACGAAGTTATCAC-3′; reverse 5′-GTGATAACT-TCGTATAATGTATGCTATACGAAGTTACAC) and LoxP–Sph I (forward 5′-CTAACTTCGTATAGCATACAT-TATACGAAGTTATGCATG-3′; reverse 5′-CATAACTT-CGTATAATGTATGCTATACGAAGTTAGCATG-3′), containing *LoxP* sequences with sticky ends were synthetically synthesized, annealed in vitro, and subcloned into Pml I and Sph I sites of the pRS406.CNS-1 vector, creating pRS406.CNS-1.*loxP*. This vector was linearized at the PflM I site, and the pop-in/pop-out method [K. Duff, A. McGuigan, C. Huxley, F. Schultz, J. Hardy, *Gene Ther.* **1**, 1 (1993)] was used to modify the retrofitted A94G6 YAC. YAC DNA was isolated at a final concentration of ~1 ng/ml and microinjected into fertilized FVB mouse eggs using standard procedures as previously described (*6*).
18. K. Wagner *et al.*, *Nucleic Acids Res.* **25**, 4323 (1997).
19. G. G. Loots, unpublished observations.
20. For FISH, slides of lymphocytes isolated from 4- to 6-week-old F1 transgenics were prepared and hybridized with two human P1's (H23 and H24) (*5*) as described [E. D. Green *et al.*, in *Mapping Genomes*, vol. 4 of *Genome Analysis: A Laboratory Manual Series*, B. Birren *et al.*, Eds. (Cold Spring Harbor Press, Cold Spring Harbor, NY, 1999), pp. 303–413].
21. Naïve CD4$^+$ T cells were sorted to >99% purity from spleen and lymph nodes of transgenics (6 to 8 weeks old) on the basis of small forward- and side-scattering characteristics and CD4$^+$, CD62L$^{hi}$ phenotype. Cells were activated using irradiated antigen-presenting cells with monoclonal antibodies against β T cell receptor and CD28 with IL-2; for Th1 conditions, recombinant murine IL-12 and antibody to IL-4 were used, and for Th2 conditions, recombinant murine IL-4 was used.
22. D. J. Fowell *et al.*, *Immunity* **11**, 399 (1999). At periods from 2 to 7 days, CD4$^+$ T cells were analyzed with flow cytometry (positive cells were gated as compared to isotype antibody controls and are based on at least 10,000 flow cytometric events) for expression of the designated murine and human cytokines by intracellular cytokine detection after 4 hours of restimulation with phorbol myristate acetate and ionomycin (PMA/IONO) (*4*). Supernatants from activated T cells were collected (either 72 hours after the primary stimulation with antibodies and irradiated antigen presenting cells or 24 hours after restimulation of 7-day-old cultures with PMA/IONO) and analyzed with enzyme-linked immunosorbent assay (ELISA) for human IL-5 and murine IL-13.
23. Total RNA was isolated with RNA-STAT-60 (TEL-TEST"B"). Five micrograms of RNA was reverse-transcribed into cDNA (Superscript *II*, Gibco), and expression levels were measured with TaqMan Syber-Green quantitative PCR assay (PerkinElmer). The sequences of the TaqMan primer pairs used to quantify mRNA are as follows: human IL-4 forward, 5′-ACAGCCTCA-CAGAGCAGAAGACT-3′; human IL-4 reverse, 5′-GT-GTTCTTGGAGGCAGCAAAG-3′; human IL-5 forward, 5′-ATAAAAATCACCAACTGTGCACTGAA-3′; human IL-5 reverse, 5′-CAAGTTTTTGAATAGTCTTTCCACAG-TAC-3′; human IL-13 forward, 5′-CAGAAGCTCCGC-TCTGCAAT-3′; human IL-13 reverse, 5′-ACACGTT-GATCAGGGATTCCA-3′; human KIF3A forward, 5′-CGCAGTCTCGAGAGCGTCAA-3′; human KIF3A reverse, 5′-ACACCGGGTGCGCAGA-3′; human RAD50 forward, 5′-TGTTGGCTGGCAGGATCTTT-3′; human RAD50 reverse, 5′-CGTGAGACCCGCGAATCT-3′; mouse glyceraldehyde phosphate dehydrogenase (mGAPDH) forward, 5′-GGCAAATTCAACGGCACA-GT-3′; and mGAPDH reverse, 5′-CCTCACCCCATTT-GATGTTAGTG-3′.
24. R. M. Locksley and Z. E. Wang, unpublished observations.
25. K. A. Frazer, unpublished observation.
26. We thank A. Nyugen, W. Dean, and K. Lewis for DNA sequencing; J. F. Cheng for isolating mouse chromosome 11 BACs; K. Frankel for assistance with sequence assembly; K. U. Wagner for providing the Cre recombinase transgenic mice; I. Plajzer-Frick for assistance with FISH; C. McArthur for flow cytometry; and K. Peterson and M. Dunaway for critical reading of the manuscript. Supported by the following grants: U.S. Department of Energy contract DE-AC0376SF00098, NIH GM-5748202 (K.A.F.), Howard Hughes Medical Institute, AI30663 and NIH HL56385 (R.M.L.), and National Library of Medicine LM05110 (W.M.).

12 November 1999; accepted 22 February 2000

# Specialized Fatty Acid Synthesis in African Trypanosomes: Myristate for GPI Anchors

**Yasu S. Morita, Kimberly S. Paul, Paul T. Englund***

**African trypanosomes, the cause of sleeping sickness, need massive amounts of myristate to remodel glycosyl phosphatidylinositol (GPI) anchors on their surface glycoproteins. However, it has been believed that the parasite is unable to synthesize any fatty acids, and myristate is not abundant in the hosts bloodstreams. Thus, it has been unclear how trypanosomes meet their myristate requirement. Here we found that they could indeed synthesize fatty acids. The synthetic pathway was unique in that the major product, myristate, was preferentially incorporated into GPIs and not into other lipids. The antibiotic thiolactomycin inhibited myristate synthesis and killed the parasite, making this pathway a potential chemotherapeutic target.**

*Trypanosoma brucei* causes human sleeping sickness and livestock disease in Africa. The bloodstream form of this parasite covers its surface with ~$10^7$ identical molecules of a glycosyl phosphatidylinositol (GPI)–anchored variant surface glycoprotein (VSG). The VSG GPI contains the fatty acid myristate (14:0) as its lipid moiety (*1*), and fatty acid remodeling reactions incorporate these myristates into the GPI precursor (*2*). Despite the large requirement for myristate, this fatty acid is not abundant in host bloodstreams (*3*), and the trypanosome was believed to be unable to either synthesize fatty acids de novo or to shorten longer fatty acids by β oxidation (*4*). This dilemma (*5*) provided a rationale for our investigation of fatty acid metabolism in trypanosomes. In studies on the cultured bloodstream form of *T. brucei* (*6*), we found that the elongation of laurate (12:0) to myristate was highly efficient, whereas the elongation of myristate to palmitate (16:0) was inefficient. We wondered why trypanosomes have a mechanism for the elongation of laurate, as there is little laurate in host bloodstreams (*3*) or in the parasite (*7*). We considered the possibility that trypanosomes can actually synthesize fatty acids de novo and that the elongation of laurate is a step in this pathway.

To test this hypothesis, we established a trypanosome cell-free fatty acid synthesis sys-

Department of Biological Chemistry, Johns Hopkins Medical School, Baltimore, MD 21205, USA.

*To whom correspondence should be addressed. E-mail: penglund@jhmi.edu

tem (*8*). We found maximal activity in a membrane fraction. Fatty acid synthesis requires a primer [often acetyl–coenzyme A (CoA)], malonyl-CoA as a two-carbon unit donor, and reduced nicotinamide adenine dinucleotide phosphate (NADPH) as a reducing agent. We used [$^{14}$C]malonyl-CoA as a radiolabel. As shown in an autoradiograph of a thin-layer chromatography (TLC) plate (Fig. 1A), we discovered synthesis of $^{14}$C-labeled fatty acids in bloodstream-form trypanosomes that depends on butyryl-CoA rather than acetyl-CoA as a primer.

We then compared an extract from bloodstream trypanosomes to one from procyclic forms. Procyclic forms, which reside in the insect vector, are known to synthesize fatty acids (*9*). Indeed, we found that the rate of [$^{14}$C]malonyl-CoA incorporation in procyclic extracts was 5.3 times higher than that in bloodstream-form extracts (Fig. 1B). Evaluation of the chain length of the de novo–synthesized fatty acids indicated that myristate was the predominant product in bloodstream extracts, whereas procyclic extracts synthesized more hydrophobic species (Fig. 1C). We found that the major product in bloodstream trypanosomes was insensitive to catalytic hydrogenation or silylation (*10*), which suggests that this product was not an α,β-unsaturated or β-hydroxylated species that comigrated with myristate on our TLC system. All these results show that bloodstream trypanosomes can synthesize fatty acids and that the major product is myristate.

To examine whether de novo–synthesized myristate can serve as a substrate for GPI remodeling (Fig. 2A), we initiated GPI biosynthesis in the cell-free system by adding uridine 5′-diphospho-*N*-acetylglucosamine (UDP-GlcNAc) and guanosine 5′-diphosphate (GDP)–[$^{3}$H]mannose (*11*). As expected, we found accumulation of glycolipid θ, the first intermediate of the remodeling pathway (at time 0, Fig. 2B) (*2*). When we added myristoyl-CoA to initiate remodeling, glycolipid θ was rapidly converted to glycolipid A″ and then to θ′, A, and C (*2*) (Fig. 2B). When we replaced myristoyl-CoA with a combination of butyryl-CoA, malonyl-CoA, and NADPH, we observed a similar conversion of θ to myristoylated GPIs. Remodeling depended on the addition of all three substrates for fatty acid synthesis (*6*). Additionally, we found incorporation of radioactivity from [$^{14}$C]malonyl-CoA into GPIs, and subsequent treatment with phosphatidylinositol-specific phospholipase C released radiolabeled diacylglycerol as expected (*6*).

To confirm our in vitro findings, we next determined whether trypanosomes can synthesize myristate in vivo and then use it for GPI remodeling. We found inefficient labeling of trypanosome lipids with [$^{3}$H]acetate or [$^{14}$C]butyrate, due apparently to poor uptake of the precursors into the cell (*6*). To circumvent this problem, we used the medium chain fatty acids [$^{3}$H]caprylate (8:0) and [$^{3}$H]laurate (12:0) as metabolic precursors for fatty acid synthesis, because these more hydrophobic species can efficiently diffuse through a lipid bilayer (*12*). Although trypanosomes incorporated less [$^{3}$H]caprylate and [$^{3}$H]laurate relative to [$^{3}$H]myristate (possibly due to less efficient conversion to acyl-CoAs), the pattern of lipid labeling by these precursors resembled that of [$^{3}$H]myristate (Fig. 3A) (*13*). A major fraction of radioactivity (49 to 79%) was incorporated into GPIs [that is, VSG (*6*) and glycolipids A and C (Fig. 3A)]. This preferential labeling of GPIs is remarkable, considering that free GPIs constitute substantially less than 1% of total cellular phospholipids (*14*). In contrast, [$^{3}$H]palmitate (16:0) did not label GPIs but instead labeled conventional phospholipids (Fig. 3A). To verify that the [$^{3}$H]caprylate or [$^{3}$H]laurate was elongated to myristate before incorporation into GPIs, we analyzed the chain length of total radioactive fatty acid incorporated into the cell. Nearly all of the [$^{3}$H]caprylate and [$^{3}$H]laurate was converted to myristate, whereas elongation of myristate or palmitate was not detectable (Fig. 3B). Thus, the de novo–synthesized myristate is preferentially incorporated into GPIs.

We next examined the effect of the fatty acid synthetase inhibitors cerulenin and thiolactomycin (Fig. 4A). Cerulenin inhibits the condensation step of both eukaryotic and bacterial fatty acid synthetases (*15*), usually with a median inhibitory dose ($IC_{50}$) less than 100 μM. At first glance, cerulenin seemed to have little effect on the cell-free synthesis of [$^{14}$C]malonyl-CoA–labeled fatty acids at concentrations up to 1 mM (Fig. 4B). However, with increas-

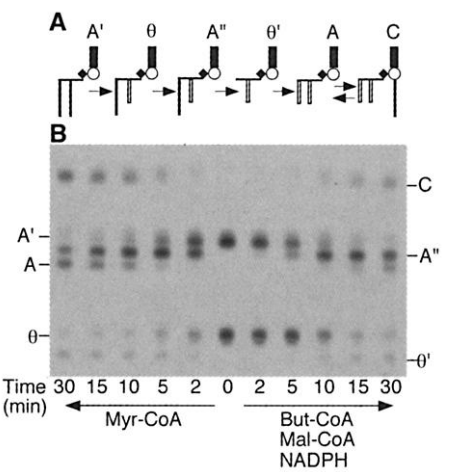


**Fig. 2.** Incorporation of de novo–synthesized myristate into GPIs. (**A**) Scheme for fatty acid remodeling. Open rectangles, myristate; vertical lines, fatty acid longer than myristate; horizontal lines, glycerol; diamonds, phosphate; circles, inositol; black rectangles, remainder of core glycan. Glycolipid A is the precursor transferred to VSG. Glycolipid C is inositol-acylated and is in equilibrium with A (*23*). (**B**) For GPI core glycan synthesis, membranes were incubated with 1 mM UDP-GlcNAc and 4 μCi/ml GDP-[3,4-$^{3}$H]mannose (DuPont, 20 Ci/mmol) for 5 min, followed by a 5-min chase with 1 mM nonradioactive GDP-mannose. $MnCl_2$, inhibitory to remodeling, was then removed by centrifugation. Myristoyl-CoA (50 μM) or a mixture of 50 μM butyryl-CoA, 50 μM malonyl-CoA, and 2 mM NADPH (concentrations are final) was then added to initiate remodeling. For extraction of GPIs, an *n*-butanol-water partition was conducted after chloroform/methanol/water (10:10:3) extraction. A portion of the TLC plate [Rf (migration relative to solvent front), 0.18 to 0.62] is shown.

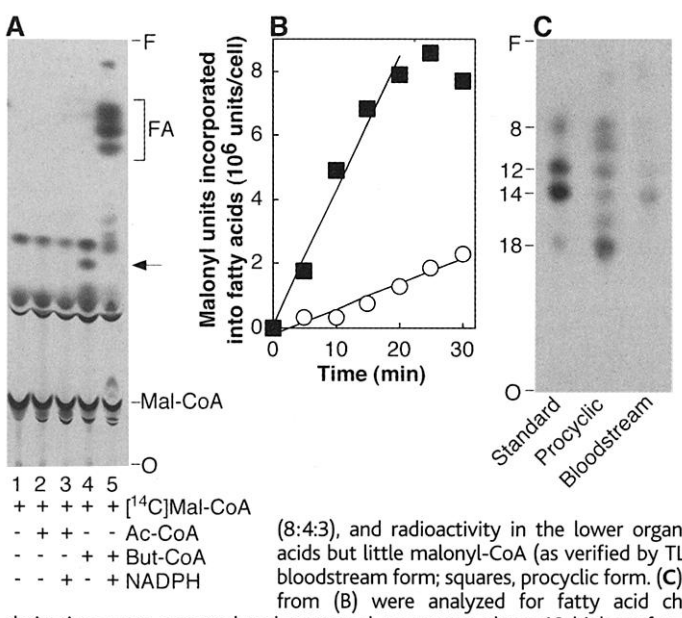


**Fig. 1.** Fatty acid synthesis in a cell-free system. (**A**) Bloodstream cell membranes were incubated with 71 μM [$^{14}$C]malonyl-CoA ([$^{14}$C]Mal-CoA), 200 μM acetyl-CoA (Ac-CoA) or butyryl-CoA (But-CoA), and 2 mM NADPH for 20 min. O, origin; F, solvent front; FA, fatty acids. The species marked with an arrow is probably β-ketohexanoic acid; other unmarked species were not characterized. (**B**) Time course of fatty acid synthesis. Lipid extracts were partitioned in chloroform/methanol/water (8:4:3), and radioactivity in the lower organic phase, containing fatty acids but little malonyl-CoA (as verified by TLC), was measured. Circles, bloodstream form; squares, procyclic form. (**C**) Lipids extracted at 30 min from (B) were analyzed for fatty acid chain length. Methyl ester derivatives were prepared and separated on reverse-phase-18 high-performance TLC (HPTLC) (Analtech) (*21*) with modifications to maximize extraction of medium chain fatty acids (*22*). Numbers at left indicate the number of carbon atoms as follows: 8, caprylate; 12, laurate; 14, myristate; 18, stearate.

ing cerulenin concentration, trypanosomes accumulated [$^{14}$C]caprate (10:0) rather than the normal end product myristate (Fig. 4C), which suggests a block in the final steps of myristate synthesis. Next we tested thiolactomycin, an antibiotic that inhibits the condensation step of the bacterial (but not eukaryotic) fatty acid synthetases (*15*). Thiolactomycin effectively inhibited trypanosomal fatty acid synthesis in vitro with an $IC_{50}$ of ~150 μM (Fig. 4B). Furthermore, thiolactomycin inhibited cell growth in culture in the same concentration range as that needed to inhibit fatty acid synthesis in vitro (Fig. 4D), which is consistent with the possibility that the in vivo target of thiolactomycin is indeed the fatty acid synthetase.

All these results demonstrate that bloodstream trypanosomes express a fatty acid synthetase. The enzyme is atypical of eukaryotic enzymes in that it produces myristate rather than palmitate, is membrane-associated rather than cytosolic, and is sensitive to thiolactomycin. This pathway resolves the dilemma that trypanosomes require more myristate than is available for salvage from the host bloodstream (*5*). Using the rate of myristate synthesis in the cell-free system (Fig. 1B), we estimate that de novo synthesis can account for at least 25% of the total requirement for myristate, with the rate in vivo potentially being much higher. Preferential incorporation of newly synthesized myristate into GPIs (Fig. 3A) is especially striking because syntheses of bulk phospholipids and GPIs both occur in the endoplasmic reticulum (ER). In the related organism *Leishmania mexicana*, GPI biosynthesis appears to occur in a subcompartment of the ER (*16*). The preferential use of de novo–synthesized myristate in GPI remodeling may imply the presence of a similar ER subcompartment in trypanosomes that contains the pathways for myristate synthesis and GPI myristoylation, but not that for conventional phospholipid synthesis.

Antitrypanosomal drugs are desperately needed. Because GPI myristoylation does not occur in mammals, this pathway could be a chemotherapeutic target. In fact, some myristate analogs are selectively toxic to trypanosomes (*17*). We now find that thiolactomycin may affect GPI remodeling by inhibiting the synthesis of myristate. Thiolactomycin has low toxicity in mice (*18*) and protects them against some bacterial infections (*19*), making this compound a promising lead for antitrypanosomal drug development. Finally, a recent finding that thiolactomycin inhibits growth of the malaria parasite (*20*) raises the possibility that fatty acid synthesis can be a versatile drug target in diverse parasitic infections.

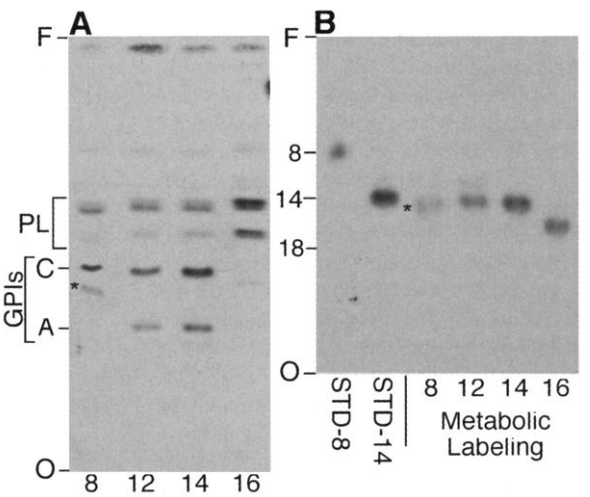


**Fig. 3.** Metabolic labeling with [$^3$H]fatty acids in infected blood. (**A**) Lipid extracts loaded on each lane of an HPTLC plate (Merck) contained 5000 dpm and corresponded to 1.0 × $10^7$ cells per lane for [$^3$H]caprylate, 2.9 × $10^5$ cells per lane for [$^3$H]laurate, 1.6 × $10^5$ cells per lane for [$^3$H]myristate, and 4.4 × $10^5$ cells per lane for [$^3$H]palmitate. PL, phospholipids. (**B**) Chain length analysis (as described in Fig. 1C) of the lipid extracts shown in (A). Standard (STD) lanes indicate authentic saturated [$^3$H]fatty acid methyl esters with indicated chain length. Aberrant migrations of [$^3$H]caprylate-labeled glycolipid A [(A), asterisk] and methyl myristate [(B), asterisk] are due to excessive cell equivalents loaded onto these lanes. Upon subsequent TLC purification, these species comigrated with authentic glycolipid A and methyl myristate (*6*).

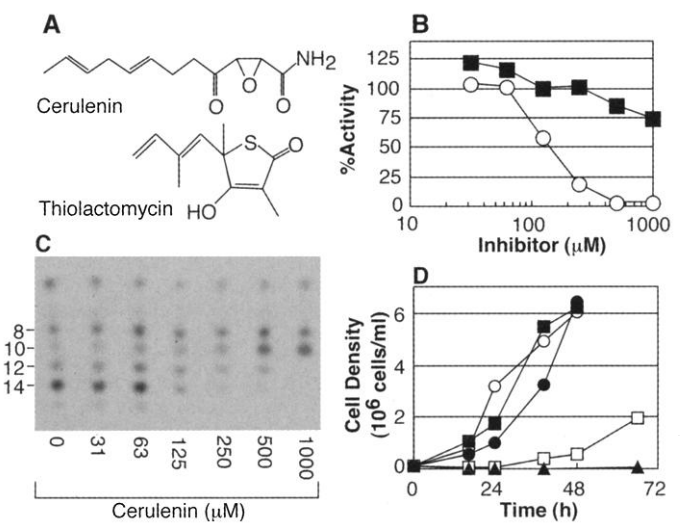


**Fig. 4.** Inhibition of fatty acid synthetase by cerulenin and thiolactomycin. (**A**) Structures of the drugs. (**B**) Effect of cerulenin (squares) and thiolactomycin (circles) on in vitro fatty acid synthesis. The cell-free system was preincubated with cerulenin (Sigma) or with thiolactomycin for 10 min at 37°C before substrate addition and another 10 min of incubation. Incorporation into lipids was measured as in Fig. 1B. (**C**) Effect of cerulenin on the product chain length, measured as in Fig. 1C. A portion of the TLC plate (Rf, 0.30 to 0.84) is shown. (**D**) Effect of thiolactomycin on live cells. Bloodstream-form *T. brucei* 427 (*24*) in HMI-9 medium (*25*) were challenged in duplicate with 0 (white circles), 62.5 (black squares), 125 (black circles), 250 (white squares), or 375 μM (triangles) thiolactomycin.


**References and Notes**

1. M. A. Ferguson, M. G. Low, G. A. Cross, *J. Biol. Chem.* **260**, 14547 (1985).
2. W. J. Masterson, J. Raper, T. L. Doering, G. W. Hart, P. T. Englund, *Cell* **62**, 73 (1990).
3. C. Edelstein, in *Biochemistry and Biology of Plasma Lipoproteins*, A. M. Scanu and A. A. Spector, Eds. (Dekker, New York, 1986), pp. 495–505.
4. H. Dixon, C. D. Ginger, J. Williamson, *Comp. Biochem. Physiol. B* **39**, 247 (1971).
5. K. A. Werbovetz and P. T. Englund, *Mol. Biochem. Parasitol.* **85**, 1 (1997).
6. Y. S. Morita, data not shown.
7. H. Dixon and J. Williamson, *Comp. Biochem. Physiol.* **33**, 111 (1970).
8. Cell lysates from the bloodstream form (strain ILTat 1.3) and the procyclic form (strain 427) of trypanosomes were prepared as described (*11*), except that tunicamycin treatment was omitted and *N*-α-*p*-tosyl-L-lysine chloromethyl ketone was omitted during the wash. Assays were conducted at 1 × $10^9$ to 5 × $10^9$ cell equivalents per milliliter in a buffer containing 50 mM Hepes (pH 7.4), 25 mM KCl, 5 mM $MgCl_2$, 5 mM $MnCl_2$, 1 mM dithiothreitol, tunicamycin (0.8 μg/ml), and leupeptin (1 μg/ml). Fatty acid synthesis was conducted with 2 mM NADPH and 50 μM each of [2-$^{14}$C]malonyl-CoA (Amersham, 56 mCi/mmol) and butyryl-CoA, unless otherwise indicated. All incubations were at 37°C. Lipids were extracted by a chloroform/methanol/water mixture (at a ratio of 10:10:3) and separated by TLC on silica gel 60 (Merck) eluted with chloroform/methanol/water (10:10:3).
9. R. A. Klein and D. J. Linstead, *Biochem. Soc. Trans.* **4**, 48 (1976).
10. K. S. Paul, data not shown.
11. W. J. Masterson, T. L. Doering, G. W. Hart, P. T. Englund, *Cell* **56**, 793 (1989).
12. F. Kamp, J. A. Hamilton, H. V. Westerhoff, *Biochemistry* **32**, 11074 (1993).
13. For metabolic labeling, blood from an infected rat (~5 × $10^8$ trypanosomes per milliliter) was incubated with $^3$H-labeled fatty acids (35 μCi per 3 ml of blood) for 45 min at 37°C with 4% $CO_2$ (*14*). Caprylate (8:0) (American Radiolabeled Chemicals) was at 20 Ci/mmol, laurate (12:0) (American Radiolabeled Chemicals) was at 60 Ci/mmol, myristate (14:0) (Amersham) was at 53 Ci/mmol, and palmitate (16:0) (DuPont) was at 43 Ci/mmol. Parasites were then separated from host blood cells (*14*), and lipids were extracted by chloroform/methanol/water (10:10:3). Animal care followed institutional guidelines.
14. T. L. Doering *et al.*, *J. Biol. Chem.* **268**, 9215 (1993).
15. K. Magnuson, S. Jackowski, C. O. Rock, J. E. Cronan Jr., *Microbiol. Rev.* **57**, 522 (1993).
16. S. C. Ilgoutz, K. A. Mullin, B. R. Southwell, M. J. McConville, *EMBO J.* **18**, 3643 (1999).
17. T. L. Doering *et al.*, *Science* **252**, 1851 (1991).
18. H. Oishi *et al.*, *J. Antibiot.* (*Tokyo*) **35**, 391 (1982).

19. S. Miyakawa, K. Suzuki, T. Noto, Y. Harada, H. Okazaki, *J. Antibiot. (Tokyo)* **35**, 411 (1982).
20. R. F. Waller *et al.*, *Proc. Natl. Acad. Sci. U.S.A.* **95**, 12352 (1998).
21. T. L. Doering, M. S. Pessin, G. W. Hart, D. M. Raben, P. T. Englund, *Biochem. J.* **299**, 741 (1994).
22. A. S. Fosbrooke and I. Tamir, *Clin. Chim. Acta* **20**, 517 (1968).
23. M. L. Güther and M. A. Ferguson, *EMBO J.* **14**, 3080 (1995).
24. G. A. Cross, *Parasitology* **71**, 393 (1975).
25. H. Hirumi and K. Hirumi, *J. Parasitol.* **75**, 985 (1989).
26. We thank A. Acosta-Serrano, D. Jiang, M. Klingbeil, D. Lane, T. Shapiro, and P. Watkins for discussions; Y. Ichikawa and V. Klein for help; and Pfizer for thiolactomycin. Supported by NIH grant AI21334.

13 January 2000; accepted 15 February 2000

# Unfolding Pathways of Individual Bacteriorhodopsins

**F. Oesterhelt,[1] D. Oesterhelt,[2] M. Pfeiffer,[2] A. Engel,[3] H. E. Gaub,[1]* D. J. Müller[3,4]**

**Atomic force microscopy and single-molecule force spectroscopy were combined to image and manipulate purple membrane patches from *Halobacterium salinarum*. Individual bacteriorhodopsin molecules were first localized and then extracted from the membrane; the remaining vacancies were imaged again. Anchoring forces between 100 and 200 piconewtons for the different helices were found. Upon extraction, the helices were found to unfold. The force spectra revealed the individuality of the unfolding pathways. Helices G and F as well as helices E and D always unfolded pairwise, whereas helices B and C occasionally unfolded one after the other. Experiments with cleaved loops revealed the origin of the individuality: stabilization of helix B by neighboring helices.**

Membrane proteins acquire their unique functions through specific folding of their polypeptide chains stabilized by specific interactions in the membrane. Their stability or resistance to unfolding, which goes hand in hand with their anchoring into the hydrophobic belt of the membrane, is usually investigated by chemical or thermal denaturation (*1, 2*). Such experiments, however, provide only ensemble information about the energetics but not about individual proteins and their anchoring forces. As described by the fluid mosaic model (*3*), membrane proteins may diffuse within the bilayer but in the normal direction are strongly restricted to the membrane plane. It is expected that stability of membrane proteins involves interactions with the lipid bilayer as well as intra- and intermolecular interactions (*1*). Thus, it is tempting to determine not only the forces that anchor membrane proteins in the membrane but also the forces that interact between their secondary structure elements.

To answer this pertinent question in membrane biology, we combined atomic force microscopy (AFM) (*4–6*) and single-molecule force spectroscopy (*7–17*) to image individual membrane proteins (*18–21*) and to measure their molecular forces. We chose bacteriorhodopsin (BR), a light-driven proton pump, because it represents one of the most extensively studied membrane proteins (*22, 23*). Structural analysis has revealed the photoactive retinal embedded in seven closely packed α-helices (*24–28*), which builds a common structural motif among a large class of related G-protein–coupled receptors (*29–32*). Moreover, BR has become a paradigm for α-helical membrane proteins in general and for ion transporters in particular (*22, 23, 33–37*). Together with adjacent lipids, BR molecules assemble into trimers, which are packed into two-dimensional hexagonal lattices, the so-called purple membrane of *Halobacterium salinarum*.

We allowed native purple membrane to adsorb onto a freshly cleaved mica surface (*38*). After being rinsed with buffer, the submolecular resolution of the cytoplasmic purple membrane surface was routinely observed (Fig. 1A) (*39*) in the fluid cell of a commercial AFM. The hexagonal arrangement of the trimeric BR molecules was clearly resolved. Although similar structures can be obtained by electron microscopy and x-ray crystallography, AFM provides structural information about individual proteins and their subunits in aqueous solution (Fig. 1A) (*40*).

After imaging, we positioned the AFM stylus over a protein and pushed it onto the protein with a contact force of ~1 nN for about 1 s. In about 15% of all cases, this resulted in firm adsorption of the protein to the tip, and force extension spectra like the one shown in Fig. 1B were recorded when we retracted the tip (in the other 85% of cases, no attractive interaction was measured upon retraction). The surface was imaged again and, in all cases, we found a vacancy at this position (Fig. 1C), confirming that extraction of a certain individual BR protein had been recorded in the force spectrum. The fine structure in the force spectra thus contains information about the unfolding process, and the last peak indicates that the extraction is completed.

This experimental protocol ensures that we select and address individual molecules, and it demonstrates the high precision and sensitivity with which we manipulate the protein. However, we do not control which part of the protein interacts with the tip, nor do we have detailed information about the nature of this interaction. In fact, the length of the extracted protein stretch as well as the shape of the force spectra were found to vary significantly, reflecting the variability of the attachment sites. We therefore restricted our data analysis to the 33% of all events in which firm binding of the protein to the tip occurred, which in addition to the imaged vacancy showed a force spectrum with a final rupture peak at the length of an unfolded and fully extended BR. This additional criterion ensures that only those spectra are analyzed in which an individual protein was extracted that was attached to the tip at the cytoplasmic COOH-terminus (see Fig. 2C). Note that 33% is also about what one would expect for random selection of the anchoring point, taking into account that the COOH-terminus covers about one-quarter of the surface of the protein and consists of more than half of all amino acids accessible on the cytoplasmic side (Fig. 4B).

We emphasize that analysis of a selected subset of events from an ensemble is a strength and not a weakness of experiments with individual proteins. In many experiments we can analyze a certain well-defined subset that is characterized by clear criteria and we can investigate correlations within the data (here the position of the last peak with details about the spectrum), which are not accessible in an ensemble average.

A selection of typical unfolding spectra is shown in Fig. 2A. In all cases there are four well-pronounced peaks in predominantly descending order. The relative positions of the second and last peaks are well correlated, but the positions and shapes of the first and the third peaks varied considerably. Superposition of 11 spectra in Fig. 2B reveals that the position of the first peak varies statistically, whereas the third peak appears to be a double peak.

The curves are the calculated force extension relations based on the model shown in Fig. 2C. If we assume that, upon pulling at the cytoplasmic COOH-terminus, helices G and F are extracted and unfolded (diffuse first peak), the protein stretch between the tip and the re-

[1]CeNS and Lehrstuhl für angewandte Physik, Ludwig Maximilians-Universität München, Amalienstrasse 54, 80799 München, Germany. [2]Max-Planck-Institut für Biochemie, Am Klopferspitz 18a, 82152 Martinsried, Germany. [3]M. E. Müller Institute for Structural Biology, Biozentrum, University of Basel, Klingelbergstrasse 70, 4056 Basel, Switzerland. [4]Max-Planck-Insitute of Molecular Cell Biology and Genetics, Pfotenhauerstrasse 108, D-01307 Dresden, Germany.

*To whom correspondence should be addressed.